

Collective Phenomena in Defect Crystals

Reimer Kühn^{1a} and Alois Würger^{2b}¹*Institut für Theoretische Physik, Universität Heidelberg**Philosophenweg 19, 69120 Heidelberg, Germany*²*Centre de Physique Moléculaire Optique et Hertzienne*, Université Bordeaux 1**351 cours de la Libération, F-33405 Talence cedex*

We investigate effects of interactions between substitutional defects on the properties of defect crystals at low temperatures, where defect motion is governed by quantum effects. Both, thermal and dynamical properties are considered. The influence of interactions on defect motion is described via a collective effect. Our treatment is semiclassical in the sense that we analyze collective effects in a classical setting, and analyze the influence on quantized defect motion only thereafter. Our theory describes a crossover to glassy behavior at sufficiently high defect concentration. Our approach is meant to be general. For the sake of definiteness, we evaluate most of our results with parameters appropriate for Li-doped KCl crystals.

I. INTRODUCTION

Interacting quantum impurities occur in various systems, such as spin glasses, magnetic systems with random couplings, and ionic crystals with substitutional defects. Spin glasses have been studied as a prominent example for systems far from thermal equilibrium. Though real spin glasses are of quantum nature, most theoretical approaches rely on classical models. Work on true quantum spin glasses has been mainly directed towards elucidating the nature of the phase transition to a frozen low-temperature state and at studying the influence of quantum fluctuations on the order parameter (for a recent review, see Ref. 1). Likewise with quantum ferromagnets.² Theoretical work has concentrated on the quantum phase transition that occurs at $T = 0$. In disordered quantum ferromagnets, additional interest stems from the fact that rare fluctuations of the disorder configurations leading to Griffiths singularities have a much stronger effect in the presence of quantum fluctuations than in the corresponding classical systems.¹ Pertinent experiments have been performed on the diluted dipolar Ising magnet $\text{LiHo}_c\text{Y}_{1-c}\text{F}_4$,³ which exhibits both, magnetic and spin glass order, depending on the concentration c of Ho ions. Agreement between experiment and theory for this system is, however, still not in a satisfactory state.

Early work on ionic crystals with substitutional impurities, such as lithium or cyanide in various alkali halides (KCl:Li, KBr:CN,...), focused on the thermal properties;^{4,5} experimental findings at high concentration indicated the relevance of the dipolar interactions⁶. More recently, sensitive echo measurements gave precise information on pairs of interacting impurities that occur at low doping⁷. At impurity concentrations of a few hundred ppm, the dipolar couplings destroy the coherent motion of the impurities⁸. Though a few questions would seem settled,⁹ the role of interaction, especially the dynamical aspects, is still controversial.¹⁰⁻¹³

At still higher concentration, one obtains mixed crystals that show glassy behavior with respect to the rotational motion of the impurities, such as $\text{KBr}_{(1-c)}(\text{CN})_c$ ¹⁴ or $(\text{MF}_2)_{(1-c)}(\text{LF}_3)_c$, with M=Ca,Sr,Ba. For this latter

example of mixed fluorite crystals,¹⁵ the coupled density of states of the impurity degrees of freedom was deduced from Raman spectra, at concentrations $c = 0.05 - 0.45$.

In the present paper, we study the consequences of interactions between substitutional defects for the low T properties of defect crystals. We are interested in describing the effects of interactions on quantized defect motion, as well as in analyzing the crossover to glassy behavior at sufficiently high defect concentration. Interactions may be of an electric dipolar nature, or mediated by elastic strain fields.

We consider N impurities that are randomly distributed on a lattice with N_0 sites. The defect concentration $c = N/N_0$ is usually much smaller than unity; the most interesting physics typically occurs in a range from $c = 10^{-5}$ to a few per cent.

The impurity Hamiltonian comprises a one-particle crystal field potential that is identical for each defect, and an interaction term that reflects the random configuration on the host lattice. The one-particle potential for a given impurity is written most conveniently in terms of local coordinates. For Li impurities in a KCl host, these coordinates could be chosen as $\mathbf{v}_i = \mathbf{R}_i - \mathbf{R}_i^0$, where \mathbf{R}_i is the impurity position at the lattice site \mathbf{R}_i^0 . Tunneling arises from degenerate minima at off-center positions of the crystal field potential $G(\mathbf{v}_i)$. The local displacement $|\mathbf{v}_i|$ is significantly smaller than the lattice constant. For other systems, the \mathbf{v}_i might describe orientational degrees of freedom of a defect molecule.

In a dipole approximation, the interaction of impurities i and j is linear in the local variables \mathbf{v}_i and \mathbf{v}_j and involves a coupling parameter J_{ij} . It may arise from electric dipole moments $\mathbf{p}_i = q\mathbf{v}_i$, or from elastic quadrupole moments; in both cases the interaction parameter J_{ij} is proportional to the inverse cube of the impurity distance $r_{ij} = |\mathbf{R}_i^0 - \mathbf{R}_j^0|$, that is $J_{ij} \sim r_{ij}^{-3}$.

In our investigation of collective effects we shall, in what follows, resort to a simplified description in terms of an effective *scalar* mean-field analysis that consists of the following approximations. (i) The dependence of J_{ij} on the relative angles of \mathbf{v}_i , \mathbf{v}_j , and $(\mathbf{R}_i^0 - \mathbf{R}_j^0)$, is simplified to two possible signs. (ii) The local coordinates

\mathbf{v}_i are replaced by the one-dimensional scalar variables v_i , the one-particle crystal field potential by $G(v_i)$, and the dipolar interaction by $J_{ij}v_i v_j$. In this scalar version, the impurity Hamiltonian takes the form

$$\mathcal{H} = \sum_i \frac{p_i^2}{2m} + U_{\text{int}}(\{v_i\}) \quad (1)$$

with

$$U_{\text{int}}(\{v_i\}) = -\frac{1}{2} \sum_{i \neq j} J_{ij} v_i v_j + \sum_i G(v_i) . \quad (2)$$

The distribution P_0 of dipolar couplings J_{ij} can be evaluated for spacings r_{ij} much larger than the lattice constant, i.e., for small impurity concentration $c \ll 1$. In a continuum approximation, the $J_{ij} \sim r_{ij}^{-3}$ scaling translates into

$$P_0(J_{ij}) = \frac{1}{2(N_0 - 1)} \frac{J_{\text{max}}}{J_{ij}^2}, \quad (3)$$

for $J_{\text{max}}/N_0 \leq |J_{ij}| \leq J_{\text{max}}$. The factor $\frac{1}{2}$ accounts for the two possible signs of J_{ij} . The upper bound J_{max} is determined by the interaction of closest neighbors,

$$J_{\text{max}} = \frac{3q^2}{4\pi\epsilon\epsilon_0 r_{\text{min}}^3} . \quad (4)$$

where we have used the form of the dipole moment $p_i = qv_i$. (Note that r_{min} is of the order of the lattice spacing.) Since we have replaced the dipolar interaction in three dimensions by the simpler expression $J_{ij}v_i v_j$, the numerical constant in (4) is to some extent arbitrary. Using a different scheme¹³ we would obtain $2/3$ instead of the factor $3/4\pi$. Because of the $J_{ij} \sim r_{ij}^{-3}$ scaling, the lower bound J_{max}/N_0 gives the coupling of impurities whose distance is of the order of the sample size. (iii) Lastly, we neglect the distance dependence of the couplings and approximate the random-site character of the defect problem by a mean field model with randomly distributed all-to-all connections. In a further simplifying step, the J_{ij} -distribution is taken to be of the Gaussian form

$$P(J_{ij}) = \sqrt{\frac{N}{2\pi J}} \frac{1}{J} \exp\left(-\frac{N J_{ij}^2}{2J^2}\right), \quad (5)$$

with zero mean $\overline{J_{ij}} = 0$ and finite second moment,

$$\overline{J_{ij}^2} = J^2/N , \quad (6)$$

which is determined in such a way that it coincides with that of the actual distribution function $P_0(J_{ij})$,

$$\int dJ_{ij} J_{ij}^2 P_0(J_{ij}) = \frac{1}{N_0} J_{\text{max}}^2 . \quad (7)$$

When putting $J^2/N = J_{\text{max}}^2/N_0$ and using $c = N/N_0$, we obtain the scaling of the parameter J with defect concentration c ,

$$J = \sqrt{c} J_{\text{max}} . \quad (8)$$

The Gaussian distribution P is roughly constant for $|J_{ij}|$ smaller than J/\sqrt{N} and vanishes rapidly for higher values, whereas the more precise function P_0 shows a power law behavior. We repeat that, with (8), their second moments are identical.

Within our scalar approximation, we take crystal symmetries into account by demanding that the one-particle potential satisfies the condition $G(v_i) = G(-v_i)$. More specifically we choose $G(v_i)$ to exhibit degenerate minima at finite displacement $v_i = \pm a$. As the simplest choice of an on-site potential with these properties we use

$$G(v) = g(v^2 - a^2)^2 . \quad (9)$$

The coupling constant g is chosen in such a way that the tunnel splitting Δ_0 for impurities moving in an isolated double well of the form (9) reproduces experimentally observed results for the lowest excitation energy of an isolated defect. E.g., in the case of ${}^7\text{Li}$ in a KCl host, one would require $\Delta_0 \simeq 1.1$ K, given a value of $a \simeq 0.7$ Å.

Due to the simplifications introduced above, the interaction energy (2) of the defect Hamiltonian has been made to resemble that of the SK spin-glass model,¹⁶ albeit one with continuous degrees of freedom rather than Ising spins. Models of this type have recently been proposed as candidates for describing low temperature anomalies of glassy and amorphous systems. Indeed, it has been shown^{17,18} that a frustrated interaction of the form considered here is able to produce a potential energy landscape comprising an ensemble of single- and double well configurations – the latter with a broad distribution of asymmetries and, in the translationally invariant case, also barrier heights, even if one starts out with single-site potentials $G(v)$ which are a-priori of single well form.

Our model of interacting impurities can be analyzed exactly within mean-field theory, i.e. a self-consistent representation of the interaction energy as a sum of effective single-site potential energies

$$U_{\text{int}}(\{v_i\}) \longrightarrow \sum_i U_{\text{eff}}(v_i) \quad (10)$$

becomes exact in the thermodynamic limit. The ensemble of effective single site potentials $U_{\text{eff}}(v_i)$ represents the potential energy landscape of the system of interacting defects. It will be found to contain *randomly* varying parameters whose distribution can be *computed*.¹⁷ By quantizing the defect motion within the collectively determined ensemble of effective single site potentials $U_{\text{eff}}(v_i)$, one finally obtains a semiclassical description of interaction effects on the behavior of quantum impurities.

We have organized the remainder of our material as follows. In Sec. II we analyze the potential energy landscape of the interacting system within mean-field theory. The analysis follows a proposal previously advocated for glasses.¹⁷ Sec. III describes the analytic solution of the mean-field theory in the weak coupling regime. Thermodynamic consequences of interaction effects are explored in Sec. IV, and simplifying features of two-state and

WKB approximations are discussed in Sec. V. Sec. VI is devoted to dynamic effects, in particular to a computation of the distribution of relaxation rates, and to an analysis of the dynamic susceptibility. We discuss our results in some detail in Sec. VII, comparing them with those of complementary approaches, and with experiments, and close with a brief summary in Sec. VIII.

II. MAPPING OUT THE POTENTIAL ENERGY SURFACE

To map out the potential energy surface of the interacting system,¹⁷ one computes the configurational free energy

$$f_N(\beta) = -(\beta N)^{-1} \ln \int \prod_i dv_i \exp[-\beta U_{\text{pot}}(\{v_i\})], \quad (11)$$

using replica theory to average over the ensemble of random J_{ij} matrices, so as to get *typical* results. The $T = 0$ limit is eventually taken to select one of the (possibly many) classical ground-state configurations of the interacting system.

As announced above, a mean-field decoupling produces a collection of *independent single-site* potentials $U_{\text{eff}}(v_i)$ with random parameters (which are comparable to randomly varying local fields in the context of spin-glasses). Technically, this decoupling within replica theory can be seen as a method for the self-consistent determination of the distribution of these random parameters.

We shall not repeat here the details of such a calculation, as they follow standard lines of reasoning¹⁹. One obtains $f(\beta) = \lim_{n \rightarrow 0} f_n(\beta)$ for the quenched free energy, with

$$nf_n(\beta) = \frac{1}{4}\beta J^2 \sum_{a,b} q_{a,b}^2 - \beta^{-1} \ln \int \prod_a dv^a \exp[-\beta U_{\text{eff}}(\{v^a\})]. \quad (12)$$

Here

$$U_{\text{eff}}(\{v^a\}) = -\frac{1}{2}\beta J^2 \sum_{a,b} q_{ab} v^a v^b + \sum_a G(v^a) \quad (13)$$

is an effective replicated single-site potential, and the order parameters $q_{ab} = N^{-1} \sum_i \langle v_i^a v_i^b \rangle$ are determined as solutions of the fixed point equations

$$q_{ab} = \langle v^a v^b \rangle, \quad a, b = 1, \dots, n, \quad (14)$$

where angular brackets denote a Gibbs average corresponding to the effective replica potential (13), and where it is understood that the limit $n \rightarrow 0$ is eventually to be taken.

We are, in what follows, going to solve the self-consistency equations only within the so-called replica symmetric (RS) ansatz for order parameters

$$q_{aa} = \hat{q}, \quad q_{ab} = q, \quad a \neq b. \quad (15)$$

The two order parameters of the RS ansatz must satisfy

$$\hat{q} = \langle \langle v^2 \rangle \rangle_z, \quad q = \langle \langle v \rangle \rangle_z, \quad (16)$$

in which $\langle \dots \rangle_z$ denotes an average over a zero-mean unit-variance Gaussian z while $\langle \dots \rangle$ without subscript is a Gibbs average generated by the effective replica-symmetric single-site potential

$$U_{\text{RS}}(v) = -J\sqrt{q}zv - \frac{1}{2}J^2\mathcal{C}v^2 + G(v). \quad (17)$$

with $\mathcal{C} = \beta(\hat{q} - q)$. The RS single site potential contains a Gaussian random variable z . A sum of single site potentials randomly drawn from the RS Gaussian ensemble (17) constitutes the mean-field representation (10) of the potential energy landscape in terms of an ensemble of effective single site potentials. Before analyzing this ensemble in greater detail, let us note its two most salient features.

First, due to a collective effect mediated by the interaction, there is a systematic deepening of the double-well crystal field potential experienced by the defects. Second, there is an induced distribution of asymmetries owing to the linear contribution to $U_{\text{RS}}(v)$. Note that the deepening of the double well potential will in particular give rise to a renormalization of the tunnel splitting: $\Delta_0 \rightarrow \tilde{\Delta}_0 < \Delta_0$, reducing the smallest excitation energy that occurs in the system of tunneling impurities. However, due to the spectrum of asymmetries there will also be a spread of excitation energies towards larger values, as we shall describe in greater detail below.

Either of the fixed point equations for \hat{q} or q above may be replaced by one for $\mathcal{C} = \beta(\hat{q} - q)$

$$\mathcal{C} = \frac{1}{J\sqrt{q}} \left\langle \frac{d}{dz} \langle v \rangle \right\rangle_z = \frac{1}{J\sqrt{q}} \left\langle z \langle v \rangle \right\rangle_z, \quad (18)$$

which turns out to acquire a finite value in the $\beta \rightarrow \infty$ -limit that is of interest to us here. The RS free energy is

$$f_{\text{RS}}(\beta) = \frac{1}{4}J^2\mathcal{C}(\hat{q} + q) - \beta^{-1} \left\langle \ln \int dv \exp[-\beta U_{\text{RS}}(v)] \right\rangle_z. \quad (19)$$

As the $\beta \rightarrow \infty$ -limit is taken, Gibbs averages generated by $U_{\text{RS}}(v)$ are dominated by the value(s) of v which minimize $U_{\text{RS}}(v)$, which we denote by $\hat{v} = \hat{v}(z)$ (displaying its dependence on the value of the Gaussian z). An immediate consequence is that $\hat{q} = q$ in this limit, provided that $q \neq 0$. The $T = 0$ fixed point equations are then

$$\hat{q} = q = \langle \hat{v}(z)^2 \rangle_z, \quad \mathcal{C} = \frac{1}{J\sqrt{q}} \left\langle \frac{d}{dz} \hat{v}(z) \right\rangle_z \quad (20)$$

with $\hat{v} = \hat{v}(z)$ minimizing $U_{\text{RS}}(v)$, i.e., to be determined as the appropriate solution(s) of

$$G'(\hat{v}) = J\sqrt{q}z + J^2\mathcal{C}\hat{v}, \quad (21)$$

the prime denoting differentiation with respect to v . The solution $\hat{v}(z)$ of (21) is a smooth function of z , except at $z = 0$ where $\hat{v}(z)$ has a jump-discontinuity, owing to the fact that among the solutions of (21) we have to choose the one corresponding to the *absolute* minimum of U_{RS} . For $z \neq 0$ then, we obtain

$$\frac{d}{dz} \hat{v}(z) = \frac{J\sqrt{q}}{G''(\hat{v}) - J^2\mathcal{C}} \quad (22)$$

Taking the jump discontinuity of $\hat{v}(z)$, hence the δ -function singularity of its z -derivative at $z = 0$ into account, we obtain the following form of the fixed point equation for \mathcal{C}

$$\mathcal{C} = \left\langle \frac{1}{G''(\hat{v}) - J^2\mathcal{C}} \right\rangle_z + \frac{\Delta\hat{v}(0)}{J\sqrt{2\pi q}}, \quad (23)$$

where $\Delta\hat{v}(0)$ denotes the size of the jump of \hat{v} at $z = 0$. The $T = 0$ limit of the free energy, i.e., the internal energy u is

$$u = \frac{1}{4} J^2 \mathcal{C} (\hat{q} + q) + \langle U_{\text{RS}}(\hat{v}(z)) \rangle_z. \quad (24)$$

Owing to symmetry, the fixed point equations always admit of a $q = 0$ solution. In a situation, where $G(v)$ is of double-well form (with minima at $\pm a$), however, only the $q \neq 0$ solution is thermodynamically acceptable as $T \rightarrow 0$. Using the fixed point equations, we find that the internal energy is given by

$$u = -J^2 \mathcal{C} \hat{q} + \langle G(\hat{v}(z)) \rangle_z. \quad (25)$$

in this limit.

III. THE LOW-CONCENTRATION OR WEAK-COUPLING REGIME

The weak-coupling (low-concentration) limit is formally defined by the inequality $J a^2 / g a^4 \ll 1$. It states that typical interaction energies are much smaller than the bare classical barrier height of the on-site potential $G(v)$. In this limit, one has approximately $\hat{v}(z) \simeq \tilde{a} \text{sgn}(z)$ for moderate values of the Gaussian z , hence $\hat{q} = q \simeq \tilde{a}^2$ and $\mathcal{C} \simeq J^{-1} \sqrt{2/\pi}$. Here $\pm \tilde{a}$ denotes the coordinates of the minima of $U_{\text{RS}}(v)$ at $z = 0$, that is

$$\tilde{a} = a \left(1 + \sqrt{\frac{2}{\pi}} \frac{J}{4g a^2} \right)^{1/2} \quad (26)$$

In the weak coupling limit, therefore, the effective single site potential experienced by the defects is of the form

$$U_{\text{RS}}(v) = -J \tilde{a} v - \frac{J}{\sqrt{2\pi}} v^2 + G(v), \quad (27)$$

exhibiting both, the systematic deepening of the double well potential experienced by the defects, and the induced distribution of asymmetries due to the linear contribution to $U_{\text{RS}}(v)$ mentioned above. Both scale linearly with J ,

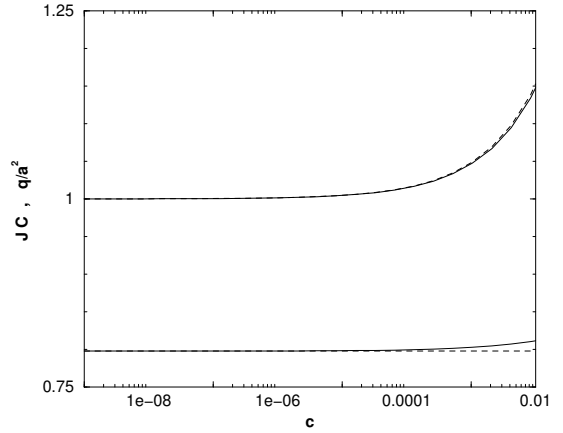


FIG. 1. Test of low-concentration approximation. Upper set of curves: q , lower set of curves: $J\mathcal{C}$, given as functions of the defect concentration c . Dashed lines give the results of the low-concentration approximation, full curves, the numerical solutions of the full fixed point equations.

hence with the square root of the defect concentration in the low concentration regime (see (8)).

As Figure 1 shows, the results of the low concentration approximation agree fairly well with those of a full numerical solution of the fixed point equations for all concentrations of interest.

IV. THERMODYNAMICS AT LOW TEMPERATURES

The contribution of the defects to the thermodynamics of the system at low temperatures is dominated by quantum effects. That is, one has to consider the quantized motion of the defects in the effective single site potentials given by (17) or by their weak-coupling approximations (27). The first task therefore consists in determining the energy levels E_n and the corresponding eigenstates ψ_n for the ensemble of effective single site Hamiltonians

$$\mathcal{H}_{\text{eff}} = \frac{p^2}{2m} + U_{\text{RS}}(v). \quad (28)$$

This done, one may proceed to compute densities of state. Normalized with respect to the total number N_0 of lattice sites, this gives

$$\rho_n(E) = c \left\langle \delta(E - \tilde{E}_n) \right\rangle_z, \quad (29)$$

where $\tilde{E}_n = E_n - E_0$. The defect contribution to the specific heat in the same normalization gives

$$C = c k_B \beta^2 \left\langle \langle \mathcal{H}_{\text{eff}}^2 \rangle - \langle \mathcal{H}_{\text{eff}} \rangle^2 \right\rangle_z, \quad (30)$$

in which now

$$\langle \dots \rangle = \frac{\text{Tr}(\dots) \exp(-\beta \mathcal{H}_{\text{eff}})}{\text{Tr} \exp(-\beta \mathcal{H}_{\text{eff}})}. \quad (31)$$

Another quantity of interest is the static (dielectric) susceptibility, originating from the interaction of the defect-dipoles with an external field \mathcal{E} , $\mathcal{H}_{\text{ext}} = -q\mathcal{E} \sum_i v_i$. The static Kubo-formula gives

$$\chi = c\beta q^2 \left\langle \left\langle v_{mm}^2 \right\rangle - \left\langle v_{mm} \right\rangle^2 \right. \\ \left. - \frac{1}{Z_{\text{eff}}} \sum_{m \neq n} \frac{e^{-\beta E_m} - e^{-\beta E_n}}{\beta E_m - \beta E_n} v_{mn}^2 \right\rangle_z. \quad (32)$$

The $v_{mn} = (\psi_n, v \psi_m)$ denote matrix elements of the position operator between the various eigenstates of the effective Hamiltonian \mathcal{H}_{eff} , and Z_{eff} is the canonical partition sum generated by it.

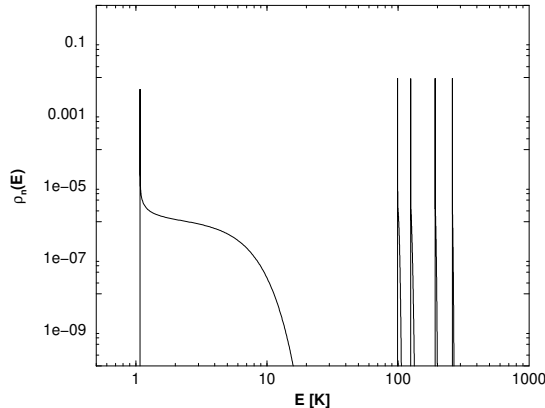


FIG. 2. Density of states for the five lowest lying excitation energies at $c = 10$ ppm

As shown in Figure 2, the lowest band of excitation energies, originating from tunneling-excitations in the ensemble of asymmetric double-well potentials extends to much lower energies than the other excitations. The latter are related to harmonic excitations about the two minima of G with energies $\hbar\omega_0$ only beyond 100 K. The pair of bands with peaks near 99 K and 125 K again corresponds to a pair of states mixed due to tunneling between the wells. The other two bands (with peaks near 192 K and 260 K correspond to states with energies above the barrier.

Tunneling excitations within the space spanned by the oscillator ground states in the two wells will dominate the low temperature physics. This is nicely seen in the specific heat data exhibited in Figure 4. Notice that the Schottky peak at low concentration is modified through interaction effects. As c is increased beyond 1000 ppm, a range of temperatures develops where the specific heat starts to show a linear temperature dependence much like in glasses. This is due to the fact that the density of states corresponding to the (lowest band of) tunneling excitations shown in Figure 2 becomes nearly constant in the energy range $\tilde{\Delta}_0 < E < \sqrt{c} J_{\text{max}} a^2$, which covers a large range of energies, as the concentration is sufficiently increased; see Figure 3 which also exhibits the renormalization of the tunneling matrix element towards lower energies due to interaction effects.

In the static susceptibility plotted in Figure 5, no significant contribution of higher order excitations is detectable (on the scale of the figure) at all, even up to temperatures as high as 60 K. The same quantity evaluated in a two-state approximation would be indistinguishable from what is shown here. Note that the concentration dependence at low temperatures is proportional to c at low concentrations, but crosses over to a \sqrt{c} behavior at larger concentrations. We shall return to this in greater detail later on.

V. TWO-STATE APPROXIMATION

At low temperatures, $k_B T \ll \hbar\omega_0$, only the two lowest lying states are significantly populated. For a sufficiently high barrier they can be constructed in terms of a basis of pocket states $|L\rangle$ and $|R\rangle$ that are localized about the potential minima at $\pm\tilde{a}$ of the two wells.

The corresponding Hamilton matrix reads

$$\mathcal{H} = \frac{1}{2} \begin{pmatrix} \Delta & \tilde{\Delta}_0 \\ \tilde{\Delta}_0 & -\Delta \end{pmatrix}, \quad (33)$$

where the off-diagonal elements are given by the renormalized tunnel energy. The diagonal entries account for an asymmetry energy between the two wells, $\Delta = [U_{\text{RS}}(-\tilde{a}) - U_{\text{RS}}(\tilde{a})]$; with (27) we find

$$\Delta = 2J\tilde{a}^2 z \equiv \bar{\Delta} z. \quad (34)$$

The two-state Hamiltonian is easily diagonalized. Its eigenvalues are given by $\pm\frac{1}{2}E$ with

$$E = \sqrt{\tilde{\Delta}_0^2 + \Delta^2}; \quad (35)$$

the corresponding eigenstates $|\pm\rangle$ may be written in terms of a mixing angle $\tan \phi = \tilde{\Delta}_0/\Delta$,

$$|+\rangle = \cos \phi |L\rangle + \sin \phi |R\rangle, \\ |-\rangle = \sin \phi |L\rangle - \cos \phi |R\rangle. \quad (36)$$

Note that the asymmetry energy Δ is linear in the Gaussian variable z ; its distribution law is thus given by

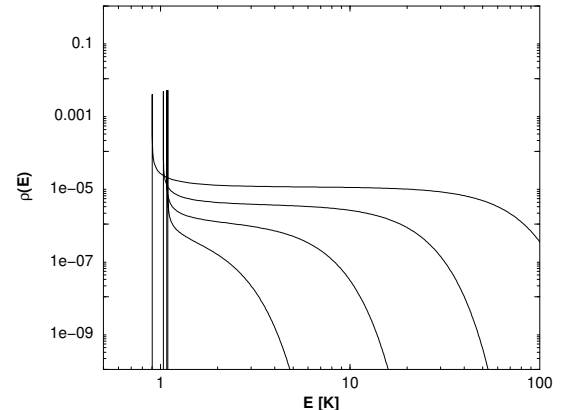


FIG. 3. Density of states for the lowest band of tunneling excitations at $c = 1, 10, 100$, and 1000 ppm (bottom to top).

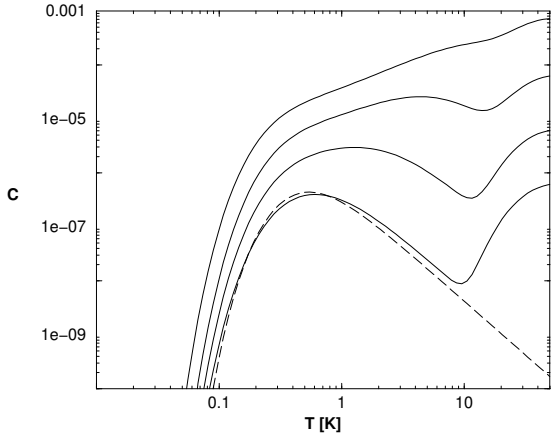


FIG. 4. Specific heat as a function of temperature for $c = 1, 10, 100$, and 1000 ppm (bottom to top). The influence of higher order excitations is seen only at temperatures above 10 K. The dashed curve is a Schottky-peak.

$$P_\Delta(\Delta) = \frac{1}{\sqrt{2\pi\Delta}} \exp\left(-\frac{\Delta^2}{2\Delta^2}\right). \quad (37)$$

As a consequence, both the two-state energy splitting E and the mixing angle ϕ are spread over a range determined by this distribution function.

The resulting density of states for the lowest band of excitation energies ($\rho(E) = \rho_1(E)$ in the notation of the previous Section)

$$\rho(E) = c \left\langle \delta\left(E - \sqrt{\tilde{\Delta}_0^2 + \Delta^2}\right) \right\rangle_z \quad (38)$$

is easily calculated. As is obvious from (35), we have $\rho(E) = 0$ for $E < \tilde{\Delta}_0$; at larger energies it is determined by the distribution of asymmetries, so

$$\rho(E) = c \frac{2E}{\sqrt{E^2 - \tilde{\Delta}_0^2}} P_\Delta\left(\sqrt{E^2 - \tilde{\Delta}_0^2}\right) \quad (39)$$

for $E \geq \tilde{\Delta}_0$, and shows a square root singularity for $E \rightarrow \tilde{\Delta}_0$; the pre-factor 2 is due the restriction $E > 0$.

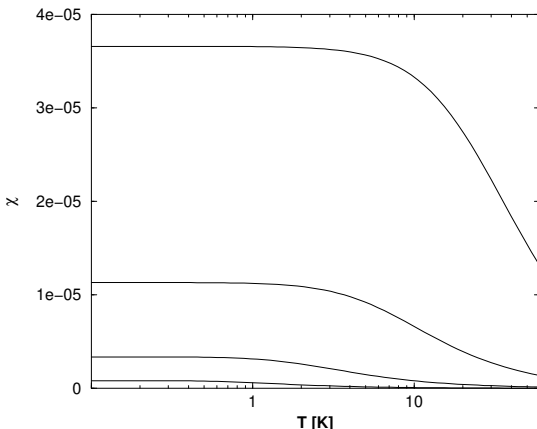


FIG. 5. Static susceptibility as a function of temperature for the same concentrations as in Figure 3.

At very low concentration, the width of $P_\Delta(\Delta)$ is much smaller than the tunnel energy $\tilde{\Delta}_0$, and $\rho(E)$ is sharply peaked about $\tilde{\Delta}_0$. As soon as the typical interaction energy $\tilde{\Delta} \simeq 2Ja^2$ exceeds the tunnel energy $\tilde{\Delta}_0$, $\rho(E)$ is well approximated by a Gaussian above $\tilde{\Delta}_0$. It remains to compute the renormalized tunnel energy $\tilde{\Delta}_0$.

With respect to the computation of $\tilde{\Delta}_0$, we have looked at two variants. In the first, both Δ_0 and its renormalized value $\tilde{\Delta}_0$ are computed exactly by solving the Schrödinger equation of the impurity moving in the appropriate crystal field potential, i.e., $G(v)$ for the former, and the renormalized potential $\tilde{G}(v) = -\frac{J}{\sqrt{2\pi}}v^2 + G(v)$ for the latter. As mentioned above, the first computation is actually used to fix the coupling g in (9) so as to reproduce the experimentally observed value — e.g., $\Delta_0 \simeq 1.1$ K for ${}^7\text{Li}$ in KCl. With parameters appropriate for the KCl: ${}^7\text{Li}$ example, this requires a potential with bare barrier height $ga^4 \simeq 174$ K.

In the second variant, both Δ_0 and its renormalized value $\tilde{\Delta}_0$ are computed within a WKB approximation. The bare tunneling matrix element is in this setting usually parameterized as

$$\Delta_0 = \hbar\omega_0 \exp(-\lambda) \quad (40)$$

with

$$\lambda = d\sqrt{2mV_B/\hbar^2}, \quad (41)$$

and parameters derived from the bare on-site potential G and the mass m of the tunneling particle — the frequency $\omega_0 = \sqrt{8ga^2/m}$ of harmonic oscillations about the minima of G , the distance $d = 2a$ between the minima, and the height $V_B = ga^4 - \hbar\omega_0/2$ of the classical barrier above ground state in the two wells. Once more, this first calculation would be used to fix the coupling constant g of the bare potential (9). Within this approximation, the classical barrier required to reproduce the bare tunneling energy reported for KCl: ${}^7\text{Li}$ is $ga^4 \simeq 84$ K, i.e. only approximately *half* the value obtained from the numerically exact analysis. The *renormalized* tunneling matrix element is computed in the same way, except that parameters are computed from the renormalized on-site potential. This gives

$$\begin{aligned} \tilde{\omega}_0 &= \omega_0 \tilde{a}/a \\ \tilde{V}_B &= V_B + \frac{1}{2} \left(\sqrt{\frac{2}{\pi}} Ja^2 + \hbar\omega_0 \left(1 - \frac{\tilde{a}}{a}\right) \right) \\ \tilde{d} &= 2\tilde{a} \end{aligned} \quad (42)$$

to lowest order in small parameters (with $\tilde{a}/a \simeq 1 + J/(4\sqrt{2\pi}ga^2)$).

The renormalized tunnel energy $\tilde{\Delta}_0 = \hbar\tilde{\omega}_0 e^{-\tilde{\lambda}}$, with

$$\tilde{\lambda} = \tilde{d}\sqrt{2m\tilde{V}_B/\hbar^2} \quad (43)$$

may thus be expressed as

$$\tilde{\Delta}_0 = \Delta_0 \sqrt{1 + \varepsilon} e^{-\delta}. \quad (44)$$

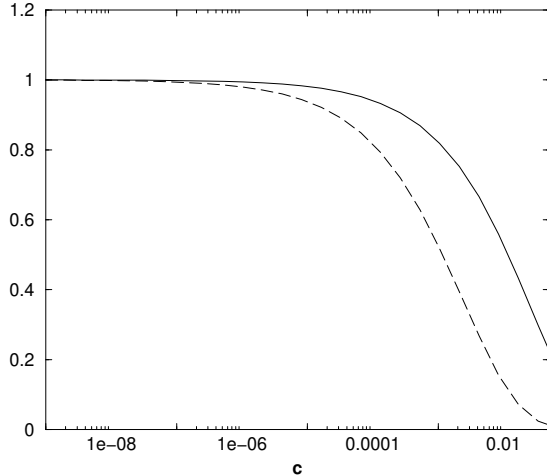


FIG. 6. The ratio $\tilde{\Delta}_0/\Delta_0$ as a function of concentration. Exact evaluation (full line), WKB approximation (dashed line).

Here

$$\varepsilon = \sqrt{\frac{2}{\pi}} \frac{Ja^2}{4ga^4} \quad (45)$$

and

$$\delta = \lambda \frac{\varepsilon}{2} \left(1 + 2 \frac{ga^4}{V_B} - \frac{\hbar\omega_0}{4V_B} \right) + \mathcal{O}(\varepsilon^2), \quad (46)$$

the latter quantity being evaluated in the weak coupling approximation, $Ja^2 \ll ga^4$ which is always appropriate for the case at hand. If, moreover, the barrier is assumed to be high, $\hbar\omega_0 \ll V_B$, so that there are many oscillator levels between the potential minima at $v \simeq \pm a$ and the top of the barrier at $v = 0$, the expression simplifies to

$$\delta \simeq \lambda \frac{3\varepsilon}{2} = \lambda \frac{3}{8} \sqrt{\frac{2}{\pi}} \frac{Ja^2}{ga^4} \simeq \sqrt{c} 3 \sqrt{\frac{2}{\pi}} \frac{J_{\max} a^2}{\hbar\omega_0}, \quad (47)$$

in which corrections involving powers of Ja^2/ga^4 and $\hbar\omega_0/ga^4$ have been neglected. There is no restriction on the ratio $Ja^2/\hbar\omega_0$. It turns out, however, that in the KCl:Li case the ratio $\hbar\omega_0/ga^4$ is roughly 1.2, thus *not* small, so that the corresponding simplifications are not available. Figure 6 compares the ratio $\tilde{\Delta}_0/\Delta_0$ evaluated numerically and via the WKB approximation (40), (41) and (44)-(46). The renormalization of the tunnel energy becomes noticeable when the concentration exceeds 100 ppm, a concentration at which the typical asymmetry Δ becomes comparable with the vibrational energy $\hbar\omega_0$ in the two wells; the renormalization effect is, however, overestimated within the WKB approximation.

In the two-state approximation, specific heat and static susceptibility are given by

$$C = c k_B \int dE \rho(E) \frac{(\beta E/2)^2}{\cosh^2(\beta E/2)}. \quad (48)$$

and

$$\chi = c \beta (q\tilde{a})^2 \left\langle \frac{(\Delta/E)^2}{\cosh^2(\beta E/2)} + 2 k_B T \frac{\tilde{\Delta}_0^2}{E^3} \tanh(\beta E/2) \right\rangle_z, \quad (49)$$

respectively. The results are valid as long as temperature is much smaller than the librational energy $\hbar\omega_0$. In (49) we have also introduced the usual approximate representation $v = \tilde{a}\sigma_z$ of the position operator in a basis of pocket states. It turns out that this latter approximation is the largest source of errors in the expression (49) for the susceptibility in that it overestimates matrix elements by roughly 10%. It turns out that this has a noticeable effect only on an overall pre-factor (at least for isolated or weakly coupled defects), but not on the temperature dependence.

VI. DYNAMICS

A. Phonon damping

The interaction of an impurity at site i with elastic waves is described by the coupling potential

$$\gamma \varepsilon v_i/a, \quad (50)$$

with the elastic deformation potential γ , the reduced coordinate v_i/a , and the phonon strain field

$$\varepsilon = \sum_{\mathbf{q},s} \sqrt{\frac{\hbar}{2V\varrho\omega_{qs}}} q_i (b_{qs} - b_{qs}^\dagger), \quad (51)$$

where ϱ is the mass density of the host crystal, and \mathbf{q} labels the wave vector of three acoustic phonon branches s . There is ample evidence that the defect-phonon coupling is weak; therefore it may be treated in first Born approximation.

All dynamic information may be obtained from the two-time correlation function

$$G(t) = (1/2\langle v^2 \rangle) \langle v(0)v(t) + v(t)v(0) \rangle, \quad (52)$$

with the normalization condition $G(0) = 1$. At low temperatures, we may use the two-state approximation. We shall here restrict ourselves to the simplified representation $v = \tilde{a}\sigma_z$ of the position operator in the basis of pocket states as introduced above; it is sufficiently precise to give qualitatively reliable results.

The theory of a weakly damped two-state system has been derived in many places; here we merely quote the result for the correlation function,

$$G(t) = \frac{\tilde{\Delta}_0^2}{E^2} \cos(Et/\hbar) e^{-\frac{1}{2}\Gamma t} + \frac{\Delta^2}{E^2} ((1-Q)e^{-\Gamma t} + Q), \quad (53)$$

with $Q = \tanh(\beta E/2)^2$ and the one-phonon damping rate

$$\Gamma = \frac{1}{2\pi} \frac{3\gamma^2}{\hbar^4 \varrho v_s^5} \tilde{\Delta}_0^2 E \coth(\beta E/2). \quad (54)$$

Here v_s denotes the sound velocity. $G(t)$ determines the linear response of a two-state system with dipole moment $p = qa\sigma_z$, tunnel energy $\tilde{\Delta}_0$ and asymmetry Δ . There are several interesting issues arising from the above model.

First, the Gaussian distribution for the bias Δ leads to a distribution of resonance energies E and relaxation rates Γ .

Second, because of the variation of the typical asymmetry $\bar{\Delta}$ with concentration c , the relaxation behavior of the impurities changes significantly with increasing c . From (53) it is immediately clear that there is no significant relaxation contribution for $\bar{\Delta} \ll \tilde{\Delta}_0$, i.e., at low concentration. In the opposite case $\bar{\Delta} \gg \tilde{\Delta}_0$, the oscillatory (resonant) part of $G(t)$ is insignificant, and the relaxation term governs the impurity dynamics.

Third, the temperature factor of the relaxation contribution, $1 - Q = \cosh(\beta E/2)^{-2}$, vanishes at very low temperatures $k_B T \ll E$, whereas it tends towards unity at higher T and large concentration.

B. Rate distribution

Recent measurements of the dielectric constant of KCL:Li revealed relaxational motion of the lithium impurities over several decades in the kHz range.⁸ Such a broad relaxation spectrum is characteristic for disordered system in general. Therefore we discuss in some detail the distribution of relaxation rates

$$P_\Gamma(\Gamma) = \frac{1}{N} \sum_i \delta(\Gamma - \Gamma_i). \quad (55)$$

In our two-state model there is only one variable, $\Delta = z\bar{\Delta}$, which is entirely determined by the Gaussian distribution of z and the constant $\bar{\Delta}$; cf. (35).

We give explicitly the rate distribution at zero temperature, because of its simplicity and since it shows the essential features. At $T = 0$, Eq. (54) gives

$$\Gamma = \frac{\tilde{\Gamma}_0}{\Delta_0} E \quad (56)$$

with

$$\tilde{\Gamma}_0 = \frac{\tilde{\Delta}_0^3}{\Delta_0^3} \Gamma_0 \quad \text{and} \quad \Gamma_0 = \frac{1}{2\pi} \frac{3\gamma^2}{\hbar^4 \varrho v_s^5} \Delta_0^3. \quad (57)$$

Hence, except for scales, the rate distribution is at the presently chosen level of description basically equivalent to the density of states in the two-level approximation. Substituting the Gaussian variable z appearing in the energy E , we find

$$P_\Gamma(\Gamma) = \frac{1}{\sqrt{2\pi}} \frac{\tilde{\Delta}_0}{\Delta_0} \frac{2\Gamma}{\sqrt{\Gamma^2 - \tilde{\Gamma}_0^2}} \exp \left[-\frac{1}{2} \frac{\tilde{\Delta}_0^2}{\bar{\Delta}^2 \tilde{\Gamma}_0^2} (\Gamma^2 - \tilde{\Gamma}_0^2) \right] \quad (58)$$

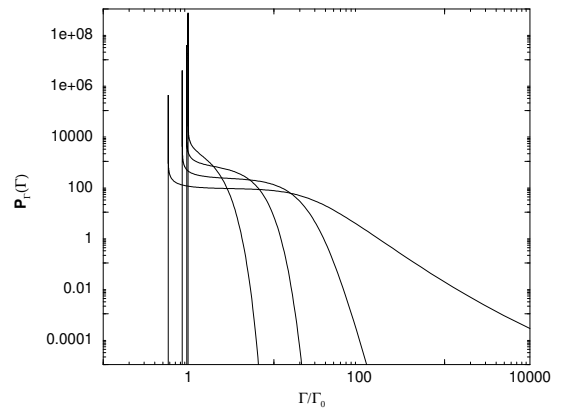


FIG. 7. Rate distribution at $T = 0$ for $c = 1, 10, 100$ and 1000 ppm.

for $\Gamma \geq \tilde{\Gamma}_0$.

Here, $\tilde{\Gamma}_0$ is the minimum rate at finite doping. According to (57), it is reduced by a factor $\tilde{\Delta}_0^3/\Delta_0^3$ as compared to the rate in the dilute limit, Γ_0 . Like the density of states, $P_\Gamma(\Gamma)$ contains a Gaussian factor and a square root singularity at the minimum value $\tilde{\Gamma}_0$. The latter is of little relevance, and the rate distribution is governed by the exponential in (58). We point out the most salient features of the rate distribution.

(i) For low impurity concentration, we have $\tilde{\Delta}_0 \gg \bar{\Delta}$, and $P_\Gamma(\Gamma)$ is a sharply peaked function with the lower cut-off $\tilde{\Gamma}_0$. In the dilute limit $c \rightarrow 0$, the distribution tends towards a delta function at Γ_0 . However, already at concentrations as low as 1 ppm, the rate distribution has a visible tail towards higher rates due to the presence of asymmetries (see Figure 7).

(ii) In the opposite case of high doping, the maximum asymmetry exceeds by far the reduced tunnel energy, $\tilde{\Delta}_0 \ll \bar{\Delta}$. As a consequence, the Gaussian factor in (58) leads to a wide distribution that is almost constant between the lower bound $\tilde{\Gamma}_0$ and the effective upper cut-off $(\bar{\Delta}/\tilde{\Delta}_0)\tilde{\Gamma}_0$.

(iii) The lower bound of the distribution, $\tilde{\Gamma}_0$, depends on the impurity concentration. In the dilute case, the tunnel energy is given by the bare value Δ_0 . Yet at finite concentration, the renormalization of the tunnel energy reduces the rate by the factor $\tilde{\Delta}_0^3/\Delta_0^3$. At $c = 0.01$, the minimum rate is by roughly one order of magnitude smaller than in the dilute case. (The WKB approximation predicts more than two orders of magnitude; see Figure 6). Thus interaction leads to both slow and very fast relaxation, as compared to the low-doping case.

Figure 7 shows the evolution from low to high doping. For concentrations up to 100 ppm, the curves have the same shape as those for the density of states (as predicted within the two-level approximation using the pocket state approximation for the position operator. The curve for 1000 ppm develops a different shape at high rates, because the pocket state representation of the position operator becomes less and less precise at large asymmetries (compare Figures 7 and 3).

C. Dynamic susceptibility

Experimental investigations of the two-state dynamics in terms of elastic or dielectric response function involve the dynamical susceptibility $\chi(\omega) = \chi'(\omega) + i\chi''(\omega)$, whose spectral function

$$\chi''(\omega) = c \frac{2}{\hbar} \tanh(\beta\hbar\omega/2) \langle G''(\omega) \rangle_z \quad (59)$$

is related to the average of the motional spectrum $G''(\omega)$, i.e. of the Fourier transform of (53). (The additional prefactor $(q\tilde{a})^2$ appearing in the susceptibility (49) and (32) is due to the fact that in Secs. III and IV we have considered an external field coupling to the *dipole operator* qv rather than to a normalized position operator $v/\sqrt{\langle v^2 \rangle}$ whose correlator is considered in (52)).

Here we give explicitly the real part that describes the sound velocity or the reactive part of the dielectric function. For relevant frequencies $\hbar\omega \ll \tilde{\Delta}_0$ (and relaxation rates at typical concentrations satisfying $\Gamma_i \ll \tilde{\Delta}_0$) one has

$$\begin{aligned} \chi'(\omega) \simeq & \frac{2}{N_0} \sum_i \frac{\tilde{\Delta}_0^2}{E_i^3} \tanh(\beta E_i/2) \\ & + \frac{\beta}{N_0} \sum_i \frac{\Delta_i^2}{E_i^2} \cosh(\beta E_i/2)^{-2} \frac{\Gamma_i^2}{\omega^2 + \Gamma_i^2} \end{aligned} \quad (60)$$

within the two-state approximation. There are two contributions of different origin to the susceptibility. The first or ‘‘resonant’’ part is dominant in the dilute limit, where the typical asymmetry is significantly smaller than the tunnel energy, $\tilde{\Delta} \ll \tilde{\Delta}_0$. On the other hand, the second contribution prevails at strong doping, where $\tilde{\Delta} \gg \tilde{\Delta}_0$.

In Fig. 8 we plot $\chi'(\omega)$ as a function of temperature for various impurity concentrations c . At low doping, the susceptibility is of the van Vleck type and hardly depends on the external frequency. The temperature variation is given by the occupation difference of the two levels, $\tanh(\tilde{\Delta}_0/kT)$; accordingly $\chi'(\omega)$ is constant for $kT < \tilde{\Delta}_0$. At larger doping, pronounced relaxational contributions occur, with peak-positions strongly dependent on frequency.

The zero-temperature value of χ' is a convenient measure of the relevance of interaction effects. The temperature factor in the relaxation contribution vanishes at $T = 0$, and one has

$$\chi' = c \frac{1}{\tilde{\Delta}_0} \langle (1 + z^2 \tilde{\Delta}^2 / \tilde{\Delta}_0^2)^{-3/2} \rangle_z. \quad (61)$$

The average over z can be written in terms of the confluent hyper-geometric function $U(a, b, x)$,

$$\chi' = c \frac{1}{\tilde{\Delta}_0} \frac{1}{\sqrt{2\nu^2}} U\left(\frac{1}{2}, 0, \frac{1}{2\nu^2}\right), \quad (62)$$

where we have defined the dimensionless coupling parameter $\nu = (\tilde{\Delta}/\tilde{\Delta}_0)$,

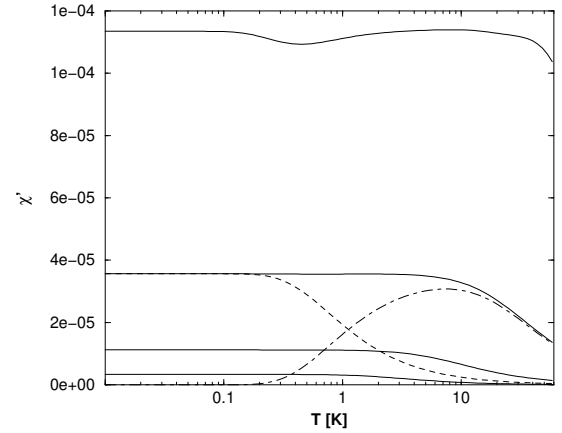


FIG. 8. Real part of the susceptibility as a function of temperature at $\omega = 10$ kHz for $c = 10, 100, 1000$ and 10000 ppm (bottom to top). For the $c = 1000$ ppm curve, the resonant (dashed) and relaxational (dot-dashed) contribution are separately exhibited as well.

$$\nu = \sqrt{c} 2 \frac{J_{\max} \tilde{a}^2}{\tilde{\Delta}_0} \simeq \sqrt{c} 2 \frac{J_{\max} a^2}{\tilde{\Delta}_0} \equiv \sqrt{\frac{c}{c_0}}. \quad (63)$$

For weak doping, the asymmetry $\tilde{\Delta}$ is much smaller than the tunnel energy; with $\nu \ll 1$ and $U(1/2, 0, 1/2\nu^2) \approx \sqrt{2}\nu$ we recover the obvious result $\chi = c/\tilde{\Delta}_0$. In the opposite case of strong doping we have $\nu \gg 1$ and $U(1/2, 0, 1/\nu^2) = u_\infty = 1.128\dots$ From (62) we thus obtain in the limiting cases

$$\chi' = \begin{cases} c/\tilde{\Delta}_0 & \text{for } c \ll c_0 \\ c/\tilde{\Delta} = u_\infty \sqrt{c c_0} / \tilde{\Delta}_0 & \text{for } c \gg c_0 \end{cases}. \quad (64)$$

The cross-over occurs at a concentration c_0 where the asymmetry attains the value of the tunnel energy, $\tilde{\Delta} \approx \tilde{\Delta}_0$, or $\nu \approx 1$. Eq. (62) yields

$$c_0 = \left(\frac{\tilde{\Delta}_0}{2J_{\max} a^2} \right)^2. \quad (65)$$

Because of the concentration dependence of $\tilde{\Delta}_0$ this is an implicit equation for c_0 . With parameters appropriate for ${}^7\text{KCl:Li}$ as used before, one finds $c_0 = \mathcal{O}(10^{-6})$; compare Figure 9.

The relaxation contribution to (60) strongly depends on the frequency ω and the rates Γ_i . Relaxation is most efficient where the rate of thermal two-level systems are close to the external frequency ω ; lowering the frequency shifts the peak to lower temperatures. The relaxation peak is significantly broadened by the rate distribution (58).

VII. DISCUSSION

A. Cross-over to relaxation

Broad spectra of energies and relaxation rates are characteristic for any disordered system. In the case of quantum impurities with dipolar interactions the broadening

is tuned by the parameter ν , which measures the strength of the interaction in units of the tunnel energy and increases with the square root of the impurity concentration c ; cf. (63).

At low doping the motional spectrum is peaked about the bare tunnel frequency Δ_0/\hbar . The relaxation rates that are close to Γ_0 as defined in (57) are of little importance, since the weight of the zero-frequency feature of the susceptibility is small. This changes as the impurity concentration reaches the value c_0 , i.e. as ν tends towards unity. Then the average asymmetry energy is comparable to the tunnel energy; as a consequence, a strong relaxation peak emerges, and both the density of states $\rho(E)$ and the rate distribution $P_\Gamma(\Gamma)$ broaden; cf. Figs. 3 and 7.

The static part of the susceptibility at $T = 0$ provides the clearest signature of this cross-over to relaxation. In Fig. 9 we compare the result of the present work (62) with that obtained previously by one of us in a Mori projection scheme¹³,

$$\chi' = \chi_0 \frac{(\sqrt{1 + \mu^2} - \mu)^2}{\sqrt{1 + \mu^2}}, \quad (66)$$

where the dimensionless coupling constant

$$\mu = c 2 \frac{J_{\max} a^2}{\Delta_0} \quad (67)$$

may be considered as the rescaled concentration. (The extra factor 2 in (67) as compared to the definition in Ref. 13 is due to the fact that our convention for the coupling between impurities differs from that used in Ref. 13 by a factor 1/2). The susceptibility in the absence of interaction, $\chi_0 = c/\Delta_0$, varies linearly with the concentration; in Fig. 9 it is indicated as a dotted line. Moreover we have indicated experimental data for various doped alkali halides.

At very low doping, both expressions (62) and (66) are linear in the concentration, as expected for non-interacting impurities, whereas at higher impurity density the dipolar interactions of the tunnel systems strongly reduce the susceptibility. We discuss the differences of the theoretical results obtained from the present mean-field model (62) and the Mori projection scheme (66).

(i) Both parameters μ and ν are proportional to the ratio of the maximum interaction $J_{\max} a^2$ and the tunnel energy. In the present approach we found a square root dependence $\nu \propto \sqrt{c}$, whereas projection scheme yields a linear law $\mu \propto c$. (Note that in the expression for ν we have neglected the weak c -dependence of $\tilde{\Delta}_0$.)

(ii) As a consequence of these different powers, the cross-over to relaxation occurs at much higher concentration in (66), $\mu \approx 1$ or $c_0 = \Delta_0/J_{\max} a^2$; the present mean-field theory yields, at $\nu \approx 1$, the square of this quantity; cf. (65).

(iii) In the strong-doping limit, the susceptibility in (62) varies as $\chi' \propto \sqrt{c}$; it still increases with concentration, whereas (66) results in a decrease, $\chi' \propto c^{-2}$.

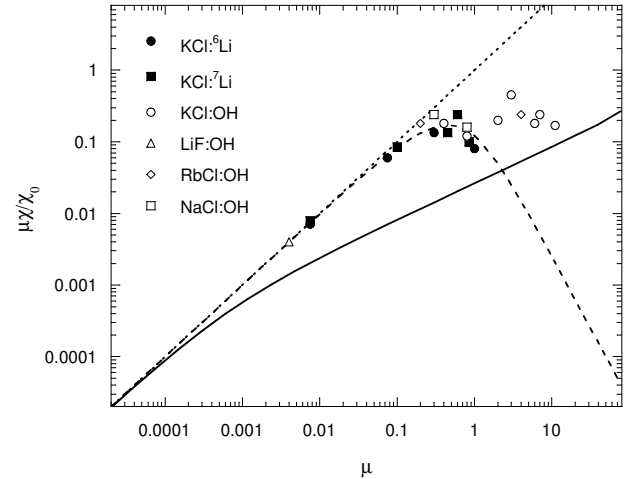


FIG. 9. Zero temperature susceptibility as a function of the concentration. The solid line gives the result of the present work, the dashed line that of Ref. 13, i.e. Eq. (66), and the dotted line indicates non-interacting impurities. Full symbols indicate experimental data on KCl:\$^6\$Li and KCl:\$^7\$Li [20, 9, 6], open symbols on KCl:OH [6, 21, 22], LiF:OH [21], RbCl:OH [6], NaCl:OH [21]. (In order to obtain comparable quantities for these various systems, we plot the rescaled susceptibility $\mu\chi/\chi_0$ as a function of the dimensionless quantity μ that is linear in c .)

These discrepancies are easily traced back to the basic assumptions of the models. The present mean-field approach relies on random couplings to *all* impurities. The characteristic interaction J is given by the second moment of the Gaussian distribution and thus is proportional to the square root of the concentration; cf. (8).

In the previous Mori approach¹³, the characteristic interaction is determined by a few nearest neighbors of a given impurity. (Because of the r^{-3} -dependence on distance of the dipolar interaction and because of its random sign, neighbors at larger distances contribute little to field at a given site.) The r^{-3} -law results in the linear variation of J with concentration.

It should be noted that the square root law (8) can be modified by a change of the mean-field model in a manner that takes the dominant effect of the interactions of a defect with a few nearest neighbors into account. In a mean-field context this might be achieved by replacing the fully connected random interaction matrix by a sparse random matrix such as in the Viana-Bray model²³, in which typical interaction scales may be chosen to scale linearly with the concentration. In the details, however, such a diluted mean-field model is much more complicated, requiring the introduction of infinitely many order parameters.

B. Comparison with experiment

The most significant result of the present work consists in the cross-over at $c = c_0$ from coherent one-particle motion to relaxation driven by the dipolar interaction. (The pre-factor $(\Delta/E)^2$ of the relaxation feature in the

susceptibility (60) vanishes for zero interaction, whereas it tends towards unity in the strong-coupling limit.)

Such a cross-over and the emergence of a relaxation peak in the motional spectrum have been observed for various impurity systems such as KCl:Li and NaCl:OH.⁹ As discussed above and shown in Fig. 9, the concentration dependence of the susceptibility in the strong-doping limit obtained in the present work, $\chi' \propto \sqrt{c}$, differs from the previous result $\chi' \propto c^{-2}$ (Ref. 13). The data for the highest concentrations ($\mu > 0.1$) clearly show the relevance of the dipolar interactions; the measured values are orders of magnitude smaller than expected for non-interacting impurities.

In spite of their marked differences of the theoretical laws (62) and (66), the available data do not permit us a definite statement on the power law $\chi \propto c^\alpha$. Though (66) provides a better fit at intermediate concentrations, $0.001 < \mu < 1$, the data do not settle the power law at high concentrations. (Unfortunately, presently available crystals do not satisfy the strong doping criterion $\mu \gg 1$.) Moreover, it is rather a difficult matter to properly separate the relaxation contribution for strongly doped crystals; thus the data points at the highest concentrations may well be too large. Further experiments at high densities would be most desirable, in view of the above discrepancy between $\alpha = \frac{1}{2}$ in the present approach and $\alpha = -2$ from Ref. 13.

We now turn to the rate distribution plotted in Fig. 7, that shows a strong broadening with rising concentration. Indeed, the relaxation spectra observed at high concentrations become very broad and develop a significant low-frequency wing⁸. On the other hand, specific heat measurements give clear evidence for a broadened density of states, in qualitative agreement with Fig. 3. (Cf. Ref. 13 and original literature cited therein.)

We close the discussion of alkali halides with a remark on the temperature dependence of the relaxation amplitude in the susceptibility (60). Since our mean-field theory reduces to a set of effective two-state systems, the relaxation feature shows the well-known factor $\cosh(\frac{1}{2}\beta E)^{-2}$ and thus vanishes exponentially in the limit $T \rightarrow 0$, whereas the rate Γ tends towards a constant. This behavior is characteristic for a local degree of freedom. The Mori projection approach, on the other hand, results in a constant relaxation amplitude and a rate that decreases at low T , thus showing the generic behavior of collective relaxation. Again, the experimental situation would seem not entirely conclusive, though the data on KCl:Li of Ref. 8 would suggest that both behaviors are present, i.e. the relaxation spectrum would comprise one-particle and collective contributions.

Finally we discuss recent Raman light scattering experiments on mixed fluorite crystals $(\text{MF}_2)_{(1-c)}(\text{LF}_3)_c$, with M=Ca,Sr,Ba.¹⁵ The reported data give strong evidence that the coupled density of states $D(E)$ of the two-level systems increases linearly with c in the range $c = 0.05 - 0.5$, i.e. $D(E) = c D_0(E)$; it would seem that the shape function $D_0(E)$ does not change in this range.

We consider very likely that the broad distribution of two-level energies observed in Ref. 15 arises from elastic

coupling of LF_3 tunneling states. In our model the TLS coupled density of states of is given by

$$D(E) = \frac{\tilde{\Delta}_0^2}{E^2} \rho(E). \quad (68)$$

With the expression (39) for $\rho(E)$ one easily finds that $D(E)$ varies over a wide range as E^{-2} and increases with c . Though these dependencies on E and c qualitatively agree with the data of Ref. 15, this experiment certainly requires a more careful study of the high-doping case. Possible discrepancies with the present description for this particular case arise from the manner in which defect crystals can, or cannot become glassy at high doping, an issue to which we now turn.

C. Crossover to glassy behavior

The appearance in our theory of a broad spectrum of excitation energies and a correspondingly broad spectrum of relaxation rates due to interaction effects at high doping is reminiscent of the physics characteristic of structural glasses. In this sense, our mean-field approach appears to describe a crossover to glassy physics at high doping. Indeed, one of the original motivations for studying defect crystals has been that they constitute systems in which – unlike in glasses – the nature of the tunneling excitations is well understood, and which at the same time offer the possibility of approaching a glassy limit by increasing the defect concentration (for a recent review, see Ref. 26). It should, however, be noted that the type of solely interaction-mediated glassiness described in the present paper is different from that believed to describe glasses proper in one essential aspect: while tunneling systems do occur with a broad distribution of asymmetries, there is – unlike in glasses – *no* corresponding randomness in barrier heights. This feature entails²⁷ for instance that the typical glassy plateau of the internal friction as a function of temperature would be absent in systems to which the present theory applies. On the other hand, such plateaus are known develop in certain defect crystals such as $(\text{CaF}_2)_{(1-c)}(\text{LF}_3)_c$, but they require defect concentrations exceeding the 10% range. There are basically two ways to create the required randomness also in the barrier heights. First, it *can* be solely interaction-mediated, if interactions are translationally invariant.¹⁸ This mechanism is, however, not available for a system of defects embedded in a crystalline host. The other possibility is to allow the crystal field potentials $G(v_i)$ to vary randomly from defect-site to defect-site. For highly doped defect crystals, this would seem like a realistic, and indeed expected feature. Unfortunately, though, there are no good theoretical models around to predict the associated kind of randomness and, in particular, its variation with defect concentration. In this sense, glassy defect crystals are apparently not much simpler systems than structural glasses proper.

D. Comparison with classical reorientation model

The dissipation rate (54) describes jumps between two quantum levels; it may be decomposed as $\Gamma = \Gamma_\uparrow + \Gamma_\downarrow$, where Γ_\uparrow accounts for thermally activated jumps from the ground state upwards and Γ_\downarrow for the reverse process. Detailed balance requires $\Gamma_\uparrow = e^{-\beta E} \Gamma_\downarrow$; thus we obtain with $E \gg kT$ the thermally activated rate

$$\Gamma_\uparrow = \tilde{\Gamma}_0 e^{-\beta E}, \quad (69)$$

where the activation energy is, in the strong-coupling limit, given by the dipolar interaction, $E = 2J\tilde{a}^2$. Such a rate, with an appropriate distribution of barrier heights, has been used in previous work on a classical reorientation model for quadrupolar glasses such as $\text{KBr}_{(1-c)}(\text{CN})_c$ ^{14,24}; in the classical picture the reorientation of the cyanide molecules (i.e. rotation by π) requires to overcome their quadrupole-quadrupole interaction that corresponds to our $2J\tilde{a}^2$. Thus the present quantum mechanical calculation yields in the classical limit the proper temperature dependence of the rates. (The present rate distribution is, however, much simpler than that derived in Ref. 24.)

VIII. SUMMARY

We have studied interacting quantum impurities in terms of a mean-field model with a Gaussian distribution for the couplings. We briefly summarize our main results.

(i) The dipolar interaction leads to a reduction of the tunneling amplitude and to a wide distribution of the asymmetry energy. As a consequence, the density of states is smeared out to both to smaller and higher values as compared to the unperturbed tunnel energy Δ_0 . Similarly, in the strong-coupling limit the relaxation spectrum covers several orders of magnitude. These features account for the collective nature of the underlying relaxation process; they are in qualitative agreement with experiments on lithium doped potassium chloride.⁸

(ii) As a clear signature of interaction effects we consider how the zero-frequency susceptibility at low T varies with the impurity concentration c . The present result, $\chi \propto \sqrt{c}$, strongly deviates from the law $\chi \propto c^{-2}$ found previously in a different approach. Though more recent experiments on KCl:Li would seem to speak in favor of this latter result,⁹ the data presently available in the strong-doping regime $\mu > 1$ do not unambiguously answer this question. Note, however, that the \sqrt{c} scaling is clearly a consequence of the ‘naive’ mean-field assumption of identically distributed all-to-all interactions. It is likely to be modified in more realistic approaches. For instance, by introducing an ad-hoc c scaling of our interaction parameters in an otherwise structurally unmodified mean-field approach, one would obtain a $c^{1/3}$ behavior of the $T = 0$ susceptibility at large doping instead of the \sqrt{c} behavior.

(iii) Since the above square root behavior results from a generic feature of the Gaussian mean-field model, an

experimental test of this law would be interesting for a wider class of models. Mean-field models with random couplings similar to that considered in this paper are frequently studied in view of quantum spin glasses and other disorder quantum systems.²⁵

(iv) Our theory describes a crossover to glassy behavior in the (restricted) sense that broad and rather flat distributions of excitation energies and relaxation times develop at high doping. We have argued that *true* glassiness will develop in defect crystals only, when mechanisms are invoked which are beyond those originating from defect interactions. As a consequence, true glassy defect crystals are almost as difficult to grasp theoretically as truly amorphous systems.

ACKNOWLEDGMENTS

Very useful discussions with C. Enss, J. Classen, S. Hunklinger, S. Ludwig, P. Nalbach, R.O. Pohl, M. Theisen, and B. Thimmel are gratefully acknowledged. We dedicate this paper to Franz Wegner on the occasion of his 60-th birthday, thanking him for numerous discussions and inspiration throughout the years.

^a E-Mail: kuehn@tphys.uni-heidelberg.de

^b E-mail: wuerger@cribx1.u-bordeaux.fr

¹ R.N. Bhatt, in: A.P. Young (ed.) *Spin Glasses and Random Fields*, (World Scientific, Singapore, 1998), p. 225

² B.K. Chakrabarti, A. Dutta, and P. Sen, *Quantum Ising Phases and Transitions in Transverse Ising Models*, (Springer, Berlin, 1996)

³ W. Wu, B. Ellman, T.F. Rosenbaum, and G. Aeppli, Phys. Rev. Lett. **67**, 2076 (1991); W. Wu, D. Bitko, T.F. Rosenbaum, and G. Aeppli, Phys. Rev. Lett. **71**, 1919 (1993)

⁴ V. Narayanamurti and R.O. Pohl, Rev. Mod. Phys. **42**, 201 (1970)

⁵ F. Bridges, Crit. Rev. Solid State Sci. **5**, 1 (1975)

⁶ A.T. Fiory, Phys. Rev. B **4**, 614 (1971); Rev. Sci. Instr. **42**, 930 (1971)

⁷ R. Weis et al., Phys. Rev. Lett. **75**, 2220 (1995); R. Weis et al., Ann. Phys. **6**, 263 (1997)

⁸ C. Enss, M. Gaukler, M. Nullmeier, R. Weis, A. Würger, Phys. Rev. Lett. **78**, 370 (1997)

⁹ A. Würger, R. Weis, M. Gaukler, and C. Enss, Europhys. Lett. **33**, 533 (1996); C. Enss et al., Phys. Rev. B **53**, 12094 (1996)

¹⁰ A. L. Burin and Yu. Kagan, Physica B **194-196**, 393 (1994)

¹¹ A. L. Burin, D. Natelson, D.D. Osheroff, Yu. Kagan, in: P. Esquinazi (ed.), *Tunneling Systems in Amorphous and Crystalline Solids*, Springer Berlin New York Heidelberg (1998)

¹² A. Würger, Z. f. Phys. B **94**, 173 (1994) and **98**, 561 (1995)

¹³ A. Würger, From Coherent Tunneling to Relaxation, Springer Tracts in Modern Physics Vol. 135, Springer Berlin Heidelberg New York (1997)

¹⁴ N.O. Birge et al., Phys. Rev. B **30**, 2306 (1984)

¹⁵ J.J. Tu and A.J. Sievers, Phys. Rev. Lett. **83**, 4077 (1999)

¹⁶ D. Sherrington and S. Kirkpatrick, Phys. Rev. Lett. **35**, 1792 (1975)

¹⁷ R. Kühn and U. Horstmann, Phys. Rev. Lett. **78**, 4067 (1997)

¹⁸ R. Kühn and J. Urmann, "Translational Invariance in Models for Low-Temperature Properties of Glasses", preprint cond-mat/9910195, J. Phys. C. (2000), in press.

¹⁹ M. Mézard, G. Parisi, and M. A. Virasoro, *Spin Glass Theory and Beyond*, (World Scientific, Singapore, 1987)

²⁰ R. Weis, PhD-Thesis, Heidelberg (1996), unpublished

²¹ D. Moy, R.C. Potter, and A.C. Anderson, J. of Low-Temp. Phys. **52**, 115 (1983)

²² W. Käenzig, H.R. Hart, and S. Roberts, Phys. Rev. Lett. **13**, 543 (1964)

²³ L. Viana and A.J. Bray, J. Phys C**18**, 3037 (1985)

²⁴ I. Kanter and H. Sompolinsky, Phys. Rev. B **33**, 2073 (1986)

²⁵ D.R. Grempel and M.J. Rozenberg, Phys. Rev. Lett. **80**, 389 (1997)

²⁶ R.O. Pohl, X. Liu, and R.S. Crandall, Current Opinion in Solid State and Materials Sci. **4**, 281 (1999)

²⁷ U. Horstmann and R. Kühn, Physica B **263-264**, 290 (1999)